Physics of Plasmas ARTICLE scitation.org/journal/php

Wakefield excitation by a powerful sub-nanosecond 28.6 GHz microwave pulse propagating in a plasma filled waveguide

Cite as: Phys. Plasmas **26**, 023102 (2019); doi: 10.1063/1.5085941
Submitted: 17 December 2018 · Accepted: 21 January 2019 ·
Published Online: 8 February 2019

Y. Cao,[1] Y. Bliokh,[1] J. G. Leopold,[1] V. Rostov,[2] Ya. Slutsker,[1] and Ya. E. Krasik[1]

AFFILIATIONS

[1]Physics Department, Technion, Haifa 32000, Israel
[2]Institute of High Current Electronics, RAS, Tomsk 634055, Russia

ABSTRACT

High-power microwave pulse generation (~1.2 GW, ~0.4 ns, 28.6 GHz) by a super-radiant backward wave oscillator (SR-BWO) and the feasibility of wakefield-excitation with this pulse in a plasma-filled waveguide are presented. The SR-BWO is driven by an electron beam (~280 keV, ~1.5 kA, ~5 ns) generated in a magnetically insulated foilless diode and propagating through a slow-wave structure in a guiding magnetic field of 8 T. The plasma produced by an array of flashboards filling a cylindrical wire-array waveguide attached at the exit of the SR-BWO is also characterized. 1D and 3D numerical simulations demonstrate that for the experimental parameters of the microwave pulse and the flashboard plasma filling the waveguide, a wakefield forms accompanied by significant periodic density modulations such that their radial location and depth can be controlled by the waveguide radius, plasma density, and microwave power.

I. INTRODUCTION

Recent progress in the generation of intense sub-nanosecond time scale microwave (MW) beams[1] exceeding hundreds of MWs opens new opportunities to study the interaction of these beams with gas or plasma. Theoretical research and numerical modeling[2–12] predict that wakefields, ionization self-channeling, acceleration of electrons, positively charged plasma, etc., may result from such interactions. Indeed, our recent research on high power (≤500 MW) and ultra-short (~0.6 ns) X-band (9.6 GHz) focused microwave beam interactions with gas[13,14] and preliminarily formed plasma[15] showed beam propagation along a distance of several Rayleigh lengths inside a channel with an over-dense plasma boundary. The latter is the result of the enhanced impact ionization of neutrals at the periphery of the beam compared to the ionization on the beam axis where the electron's oscillatory energy can exceed 10 keV. In this research, we used a super-radiant backward wave oscillator[16,17] (SR-BWO) generating a TM_{01} mode microwave pulse. The SR-BWO differs from a long-pulse ordinary relativistic BWO by a slow-wave structure (SWS) of extended length approximately twice the electron beam length. The coherent emission in the form of a short single pulse is produced by the self-bunching of the electron beam interacting with a slow spatial harmonic of the electromagnetic wave which propagates along the electron beam with a group velocity of the opposite direction to the electron velocity. The electromagnetic pulse was converted first into a linearly polarized TE_{11} mode Gaussian beam, which was then radiated by a horn antenna followed by a dielectric lens (focal distance of 9 cm) which focused it inside a Pyrex tube filled either with a neutral gas or a preliminarily formed plasma.[18]

Because of the finite efficiency of the mode converter, antenna gain, and partial reflections from the lens, only part of the generated power was concentrated in the lens focal region. These natural obstacles can be avoided if the microwave pulse exiting the SR-BWO is directly injected into a waveguide.[19] The absence of radial divergence increases the wave amplitude and, as a result, enhances the ponderomotive force.[20] For instance, the ponderomotive force, produced by a 1 GW, 28 GHz microwave pulse propagating in a circular ~0.7 cm radius waveguide, is almost 40 times larger than that realized in earlier experiements.[13–15]

In the present paper, the experimental study of a recently built SR-BWO, which generates a 28.6 GHz, ~0.4 ns, 1.2 GW microwave pulse, is presented. The parameters of a flashboard plasma source[21] and a cylindrical waveguide with walls transparent to plasma are experimentally determined and used in

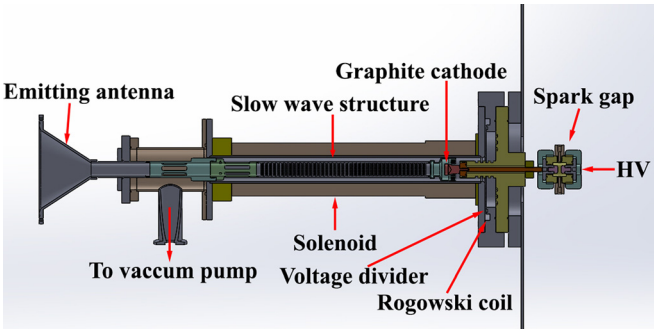

FIG. 1. Drawing of the experimental setup for generating 28 GHz high power microwave pulses by an SR-BWO.

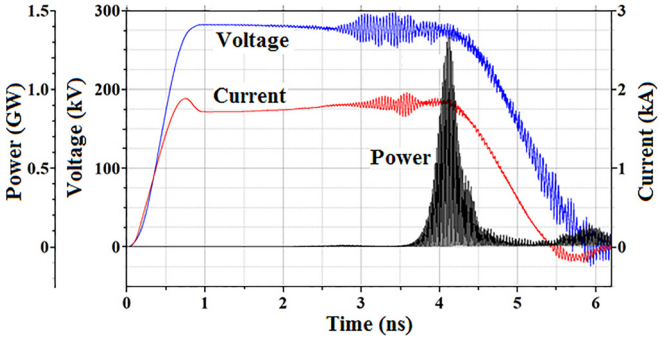

FIG. 3. 3D MAGIC-PIC simulations: The input voltage, the beam current (measured near the cathode), and the output microwave power (measured at the exit of the SR-BWO).

numerical simulations of the pulse propagation along this plasma filled waveguide.

II. MICROWAVE BEAM GENERATION IN A 28 GHz SR-BWO

A. Experimental setup and diagnostics

In Fig. 1, the experimental high-power microwave source is presented. The device consists of an all solid-state high-voltage (HV) generator based on magnetic compression stages and semiconductor opening switches[22] (not shown in Fig. 1), a magnetically insulated foilless diode with an explosive electron emitting graphite cathode,[23] a solenoid producing a guiding magnetic field sufficient for strong magnetization of the generated cylindrical electron beam, a specially designed slow wave structure (SWS), and a horn antenna.

The HV generator (internal impedance of 200 Ω), described in Ref. 23, produces at its output a negative polarity of ~320 kV and a rise-time pulse of ~2.5 ns. To reduce the rise-time to ~0.5 ns, a gas filled spark-gap switch is installed between the generator output and the cathode holder. This pulse, when applied on a 12 mm diameter sharp edged circular graphite cathode, forms an explosive emission plasma electron source,[24] generating a ~1.6 kA cylindrical electron beam. This electron beam propagates through the SWS, guided by an axial magnetic field. The magnetic field (~8 T, ~15 ms half period) is produced by an external solenoid powered by the discharge of a ~4 mF capacitor charged up to 3 kV.

The 28 GHz SWS is a corrugated wall cylindrical copper waveguide manufactured by galvano-plastics. The corrugated wall has 3 sinusoidal sections of 14, 14, and 8 periods long each respectively. The minimum radius of the SWS wall is kept constant at 6.9 mm. The amplitude of the sinusoidal corrugation grows from 0.3 mm in the first section to 0.6 mmm in the third section, whereas the period length is constant (4.8 mm). Along a final 4 period section, the corrugation is reduced to a flat surface. This design is based on the design described in Ref. 1 adjusted to the parameters of our HV generator.

Special adjustment tools were used to align the cathode, the SWS, and the solenoid tube axes. The electron beam pattern obtained on a CR-39 plastic target [Fig. 2(b)] placed at the downstream end of the SWS was used to confirm that the electron beam axis, the SWS axis, and the magnetic field were aligned within ~0.2 mm. The output of the SWS was connected to a 14 mm inner diameter cylindrical waveguide with narrow (~1 mm) longitudinal slots for vacuum pumping. The output of this waveguide was connected to a horn antenna covered by a 0.2 mm-thick Mylar interface window. We modeled the above SR-BWO design by 3D MAGIC-particle-in-cell (PIC)[25] numerical simulations for a 280 kV voltage pulse rising during 0.8 ns, producing by explosive emission a 1.7 kA electron beam, in the presence of a guiding magnetic field of 8 T (Fig. 3). An output microwave power of ~1.3 GW (non-averaged) and a pulse duration of ~0.4 ns FWHM (Full Width at Half Maximum) are predicted.

As seen in Fig. 3, oscillations in the voltage and current due to some leakage of the microwaves trough the reflector appear ~2 ns after the voltage has reached its maximum. This delay is approximately the time it takes for the beam to reach the edge of the SWS and the backward propagating wave to return to the reflector. An additional ~1 ns is required for the wave to propagate forward to the SWS output. Thus, the electromagnetic power is observed ~3 ns after the voltage rise time.

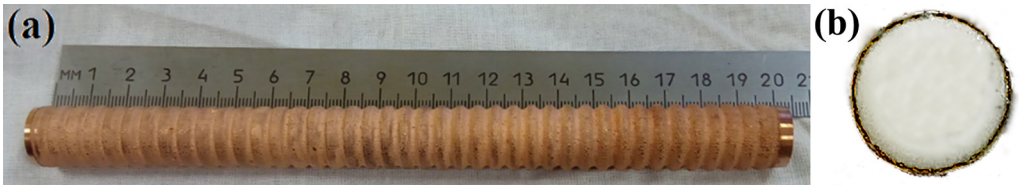

FIG. 2. (a) External view of the 28 GHz SWS and (b) the experimentally measured trace of the electron beam cross section.

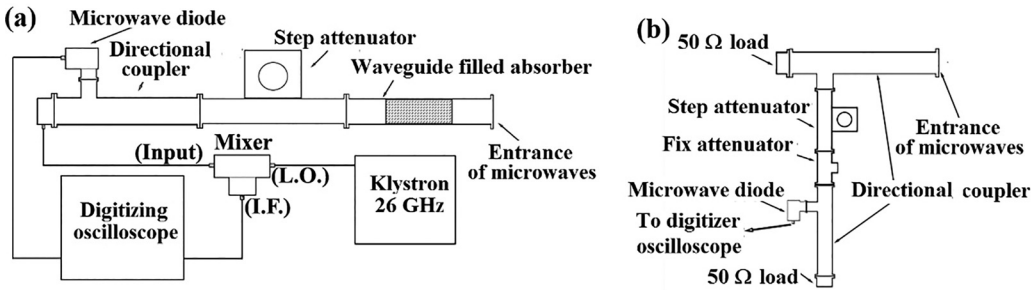

FIG. 4. (a) Microwave frequency measurement setup. (b). Microwave power profile measurement setup.

A vacuum level of ∼1.3 mPa in the foilless diode and the SWS was kept by scroll and turbo-molecular pumps. The voltage and current waveforms were measured using a capacitive voltage divider and a self-integrated Rogowski coil, respectively (see Fig. 1). The pattern of the generated microwave beam was obtained using a Canon EOS Rebel T3 digital camera operating with open shutter pointed to a screen surface covered by a matrix of miniature Ne lamps (0.5 mm diameter each) activated by the powerful MW radiation. This Ne lamp screen was placed at different distances relative to the output of the horn antenna.

The experimental arrangements for measuring the microwave beam frequency and the radial power distribution are shown in Fig. 4. The microwave beam frequency [Fig. 4(a)] was measured with the help of a double balance mixer (Marki-M9–0444) which multiplied the attenuated microwave signal with a CW signal from a Klystron oscillator operating at a frequency of 26 GHz. The signal from the "Intermediate frequency" (I.F.) port of the mixer and the rectified signal of the microwave beam obtained with a microwave diode (Milltech DXP-28) were registered using a digitizing oscilloscope. The radial distribution of the microwave power was measured by a WR-28 waveguide serving as the antenna, with a series of microwave attenuators (total attenuation of 68.2 dB) and a directional coupler with the same diode detector [see Fig. 4(b)]. The waveguide opening was placed at a distance of 20 cm from the output of the horn antenna and at different radial positions. To study the polarization of the microwaves, these measurements were performed with the waveguide oriented both vertically and horizontally. At least three shots of the generator were used for each position.

B. Microwave beam generation—Experimental results

The microwave pulse's spatial power distribution obtained by the light emission from the Neon-lamp matrix at the distances of 4 and 20 cm from the horn antenna is shown in Fig. 5. These images reflect the TM_{01} mode of the generated microwave radiation.

Typical signals obtained from the I.F. port of the mixer and Milltech DXP-28 diode are shown in Fig. 6(a). One can see that the envelopes of the two signals are similar. A Fourier transform applied to the signal obtained from the I.F. port [Fig. 6(a)] shows that the spectrum [Fig. 6(b)] has a central frequency of ∼2.6 GHz which when added to the local oscillator frequency of ∼26 GHz results in the 28.6 GHz frequency of the microwave beam. Note that the spectral width is "natural," i.e., it corresponds to the microwave pulse duration.

A typical waveform of the microwave pulse power and the results of the measurements of the radial distribution of the microwave pulse power are shown in Fig. 7. To calculate the total power, we took into account that the standard WR-28 waveguide had a coupling of −1.5 dB and that the effective area of the waveguide due to the distribution of the electric field intensity of the TE_{10} mode is $S = A \times 2/\pi$, where A is the cross-sectional area of the waveguide. By integrating the radial distribution shown in Fig. 7(b), one obtains that the SR-BWO generates a microwave pulse of ∼1.2 GW maximum power. Thus, the measured frequency, duration, and maximum power of the microwave beam agree satisfactorily with the results of the numerical simulations (Fig. 3).

III. FLASHBOARD PLASMA SOURCE: DESIGN AND CHARACTERIZATION

For studying the microwave pulse propagation through a plasma filled circular waveguide, we have developed and characterized a flashboard plasma source. We require that the plasma fills uniformly a 600 mm long region of a vacuum (several mPa) tube and that the plasma parameters can be controlled by the time delay between the plasma formation's beginning and the appearance of the microwave pulse in the waveguide. In addition, the plasma source should not interfere electromagnetically with the pulse propagation inside the waveguide. Flashboard plasma sources which have been studied in detail for many decades and widely used in research related to plasma

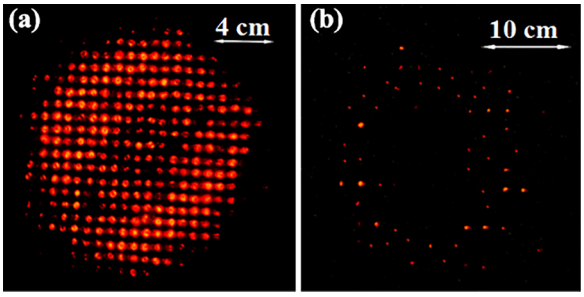

FIG. 5. (a) Microwave beam pattern at 4 cm and (b) at 20 cm from the output surface of the horn antenna.

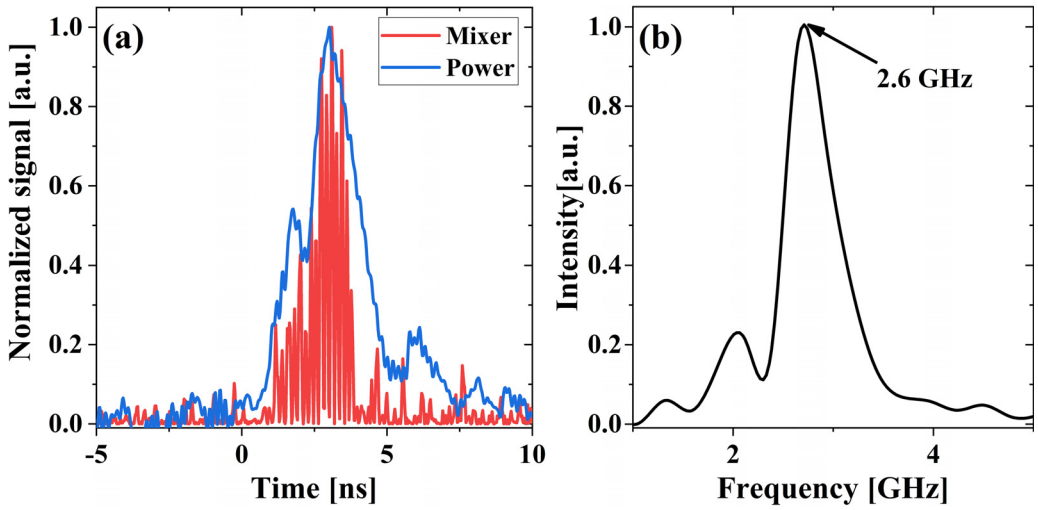

FIG. 6. (a) Waveforms of the intermediate frequency signal obtained by the mixer and by the detector (blue). (b) FFT of the intermediate frequency signal.

opening switches[21] suit all these requirements. A flashboard plasma source is a multi-electrode structure attached to a thin (a few hundreds of μm) dielectric surface with a rear solid surface grounded electrode. In our design, we have four flashboards placed inside a 700 mm long, 90 mm diameter stainless tube. The tube has two 500 mm long, 10 mm wide viewing slot windows for diagnostic purposes [Fig. 8(a)].

When a HV pulse is applied, the stray capacitors formed between each front electrode and the rear grounded electrode are charged. This is followed by a surface flashover between the front electrodes along the dielectric [Fig. 8(b)] which leads to the generation of dense current carrying plasma flows accelerated by the gradient of the self-magnetic field of the discharge current. In time, the plasma flows overlap each other and fill the entire volume of the tube. In our design, the flashboards were manufactured from printed circuit boards with 10 mm long, 6 mm wide electrodes separated by 1.5 mm gaps. The distance between electrode lines is 10 mm, and the total dimension of a single board is 300 mm (length) and 283 mm (width).

A HV pulse generator was developed and consisted of two HV, low-inductance Maxwell capacitors connected in parallel (total capacitance of 400 nF). These capacitors were charged by a 20 kV HV dc power supply and discharged using a gas spark gap switch. A trigger generator based on a HV pulse transformer was used to trigger the spark gap switch. The HV pulse generator delivers to the flashboards an output pulse of ~20 kV, ~12 kA over a period of ~1.5 μs (FWHM). In order to avoid an underdamped discharge and erratic operation of the flashboards, low-inductance resistors (total resistance of 1.5 Ω) were connected in series to each of the flashboard chain HV input points.

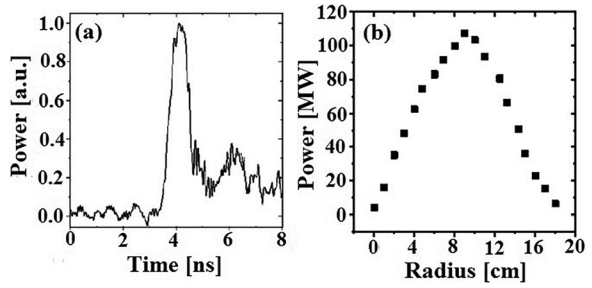

FIG. 7. (a) Typical waveform of the microwave beam power with a duration (FWHM) of ~0.4 ns. (b) Microwave power radial distribution measured at z = 20 cm.

The flashboard plasma source was characterized using various diagnostic methods. Fast intensified imaging (frame duration of 50 ns) using a 4QuikE (Stanford Computer Optics, Inc.) measured the plasma light emission's evolution viewed from the front and the side. In order to obtain the temporal development of the plasma density and the microwave cut-off, microwave interferometry and visible spectroscopy were used. The longitudinal plasma density distribution was also studied using an array of biased Faraday cups. Examples of front and side images of the plasma light emission are shown in Fig. 9. The front images [Fig. 9(a)] show that the plasma light emission first appears at the outer periphery, and in time, it fills the entire volume with maximal light intensity on axis. The latter is the result of the plasma flow converging towards the axis. The plasma light emission becomes uniform at ~90 μs. The side view images [Fig. 9(b)] confirm good longitudinal uniformity of the plasma light emission, indicating plasma uniformity.

The plasma density's temporal evolution measured by visible spectroscopy based on the Stark broadening of the H_β spectral line, the analysis of the single Langmuir probe's Ampere/Volt dependence, microwave cut-off, and interferometry are shown in Fig. 10. There is good agreement between the different diagnostic methods, showing that the flashboard plasma source is spatially uniform over a broad and controllable plasma density range (10^{10}–10^{14} cm^{-3}). A constant plasma density within this range can be chosen to fill uniformly the experimental waveguide by changing the time delay between the beginning of the plasma formation and the injection time of the microwave pulse.

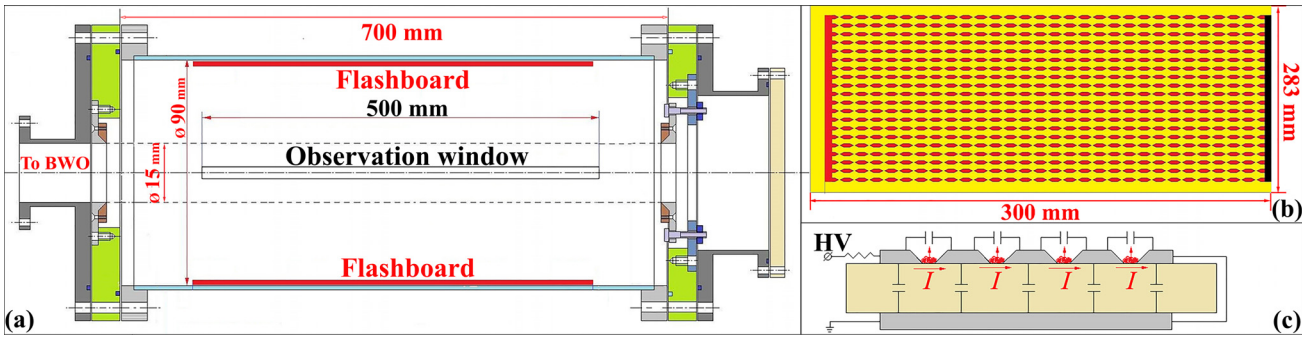

FIG. 8. (a) Drawing of the experimental chamber with the installed flashboards and (b) a flashboard and (c) its corresponding simplified equivalent electrical circuit.

Finally, we have designed a 14 mm diameter cylindrical waveguide (Fig. 11) made of thin (1 mm diameter) stainless steel wires spaced ~1 mm apart. This cylindrical wire array waveguide can be connected directly to the output of the SWS and is placed coaxially inside the vacuum tube containing the flashboards. The geometrical transparency of this waveguide is ~60%, allowing plasma to fill its entire volume. MAGIC electromagnetic simulations confirm that the microwave pulse propagation is unperturbed, and power loss is negligible in this wire array waveguide compared to its solid wall equivalent.

IV. NUMERICAL ANALYSIS OF THE WAKEFIELD GENERATED IN THE WAVEGUIDE

Recently, the propagation of an ultra-short ($\leq 10^{-9}$ s) high power (~1 GW) microwave (TM_{01} mode) pulse with a carrier frequency of 10 GHz in a cylindrical waveguide filled with an under-dense [$(2–5) \times 10^{10}$ cm^{-3}] plasma was studied both analytically and using particle-in-cell (PIC) numerical simulations.[19] It was shown that the radial ponderomotive force (quadratic in the microwave field amplitude) plays a key role in wakefield formation. The equation of electron motion in the radial direction, averaged over the fast oscillations, can be written as (see Ref. 19 for details)

$$\left\langle \frac{d\beta_\rho}{d\tau} \right\rangle = \frac{1}{2}\sin^2\psi J_1(\rho)\left\{ \underbrace{-\left[2J_0(\rho) - \frac{1}{\rho}J_1(\rho)\right]}_{\text{Ponderomotive force}} + \underbrace{\frac{1}{\cos^2\psi}J_0(\rho)}_{\text{Lorentz force}} \right\}, \tag{1}$$

where $J_0(\rho)$ and $J_1(\rho)$ are the zero and first order Bessel functions, respectively, $\beta_\rho = k_\perp v_r/\omega$, $\sin\psi \equiv k_\perp/k_0$, $\cos\psi \equiv k_z/k_0$, $\rho \equiv k_\perp r$, $k_0 = \omega/c$, $k_\perp = \gamma_{0,1}/R$, $\tau = \omega t$, ω is the frequency of electromagnetic waves, c is the speed of light, R is the radius of waveguides, and $\gamma_{0,1}$ is the first zero of the Bessel function $J_0(\rho)$. Equation (1) describes the electron motion in the absence of space charge fields. One can see that depending on the waveguide radius, the total radial force can either be in the same direction as the Lorentz force, i.e., outwards from the axis of the

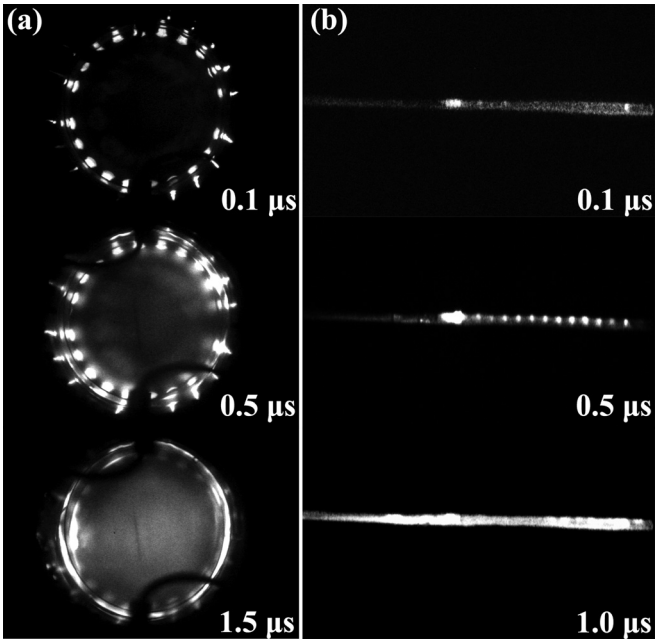

FIG. 9. Front (a) and side (b) images of the flashboard plasma light emission at various times.

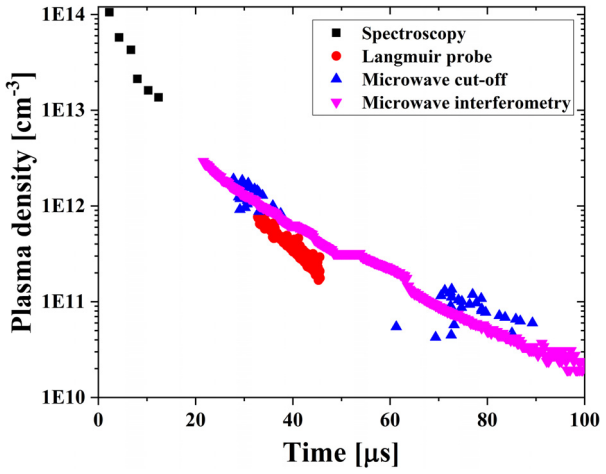

FIG. 10. Temporal plasma density dynamics measured by different diagnostic methods.

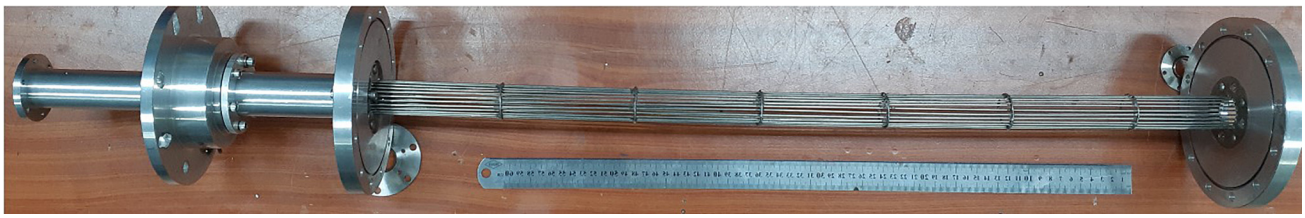

FIG. 11. External view of the cylindrical waveguide.

waveguide, or in the opposite direction forcing the electron towards the waveguide axis. The Lorentz force is always positive, i.e., forcing electrons towards the waveguide wall, while the ponderomotive (gradient) force is negative near the axis becoming positive after the maximum of $J_1(\rho)$, closer to the waveguide wall. If the Lorentz force on axis, $\rho = 0$, is larger than the gradient force, then the total radial force is positive along the entire waveguide radius. Thus, the radial force is positive everywhere, when $(\cos^2\psi)^{-1} > 1.5$. This condition defines the critical radius $r_{cr}[\text{cm}] = \sqrt{3}\gamma_{0,1}c/2\pi f = 19.85/f[\text{GHz}]$: the electromagnetic pulse forces all electrons out towards the wall for a waveguide radius r_{WG} smaller than critical, $r_{WG} < r_{cr}$. Otherwise, for $r_{WG} > r_{cr}$, some electrons are moved towards the axis and others to the waveguide wall.

In the numerical study presented below, the parameters of the microwave pulse generated in the SR-BWO, described in Sec. II, are used, that is, TM_{01} mode, 1 GW power, pulse duration less than 1 ns, and a carrier frequency of 28 GHz. It is assumed that the pulse is injected into a cylindrical waveguide filled with plasma. For these parameters, $r_{cr} \cong 6.9$ mm.

It is reasonable to assume that the MW pulse displaces plasma electrons from their equilibrium positions, while the ions remain immobile. When the pulse traverses the waveguide, the electric field of the separated charges tends to move the electron to their initial positions. Due to inertia, the electrons pass

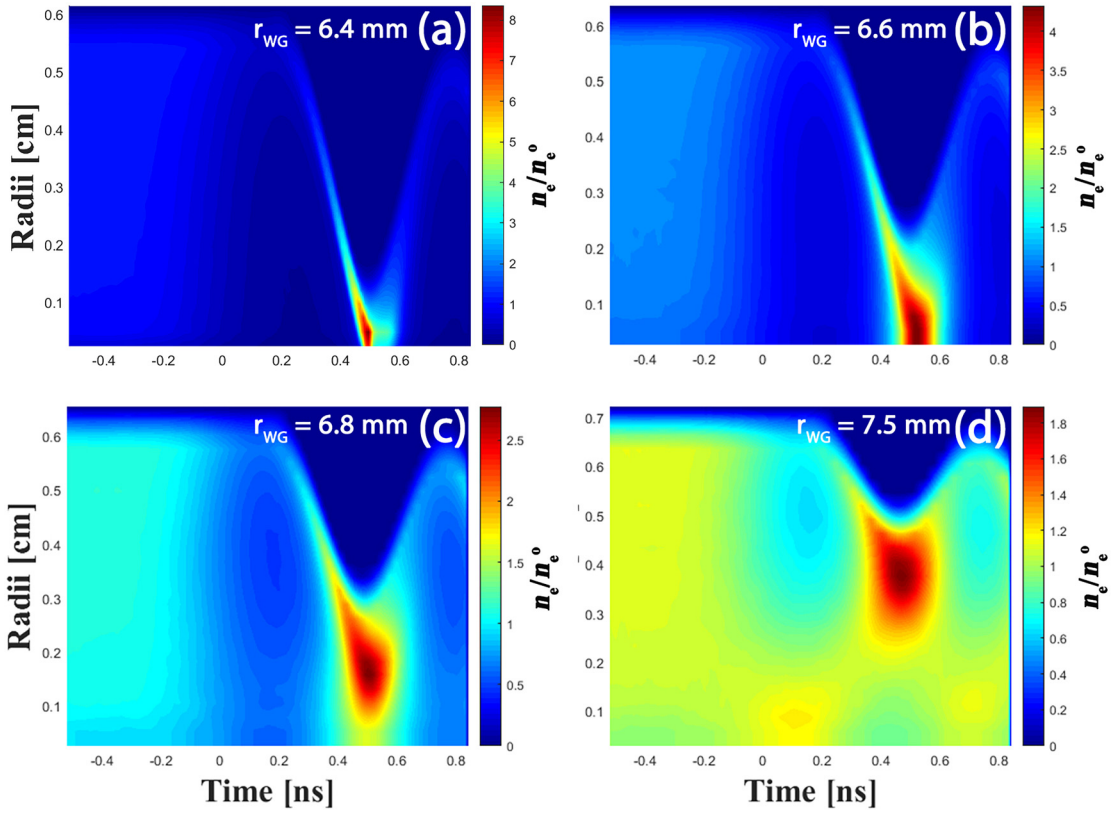

FIG. 12. Time dependent evolution of the normalized electron density for different waveguide radii. The initial plasma density is $n_e^0 = 2.5 \times 10^{10}\,\text{cm}^{-3}$, the microwave power $P = 500$ MW, and the frequency $f = 28$ GHz and 0.35 ns (FWHM) pulse duration. The time $t = 0$ corresponds to the center of the Gaussian pulse.

the equilibrium position and are focused either near the axis [Figs. 12(a) and 12(b)], when $r_{WG} < r_{cr}$, leading to significant density modulation, or somewhere between the axis and the wall [Figs. 12(c) and 12(d)] for $r_{WG} > r_{cr}$. The structure of the wakefield can be controlled by the value of the waveguide radius.

The radial distribution of the electron density, normalized to its initial value, $n_e(r)/n_e^0$, in waveguides of different radii, is presented in Fig. 13(a). One can see that the increase in the waveguide radius leads to displacement of the electron density maximum from the axis towards the wall due to the competition between the ponderomotive and Lorentz forces.

The dependence of the normalized maximum electron density n_e^{max}/n_e^0 on the waveguide radius r_{WG} is shown in Fig. 13(b) for microwave pulses of 0.5 GW and 1 GW power, propagating through plasmas of initial densities of $2.5\times10^{10}\,cm^{-3}$ and $5\times10^{10}\,cm^{-3}$. The electron density modulation, produced by a 0.5 GW pulse, reaches its maximum $n_e^{max}/n_e^0 \approx 8$ at a waveguide radius of 6.4 mm, smaller than critical, and decreases as the radius grows [red circles in Fig. 13(b)]. Increasing the microwave power from 0.5 GW to 1 GW shifts the waveguide radius where the maximum electron density modulation occurs to 6.8 mm [blue triangles, Fig. 13(b)]. The reason for this is that for small waveguide radii, a more powerful pulse forces plasma electrons towards the wall where electrons disappear so that the wakefield modulation on axis is smaller. Increasing the waveguide radius decreases the microwave power density and reduces the absorption of the plasma electrons by the waveguide wall. The use of more powerful microwave pulse allows one to obtain a strong electron density modulation during its propagation through more dense plasma [Fig. 13(b), black squares], which makes experimental measurements easier.

The numerical analysis presented above was obtained using the 1D model described in Ref. 19 and, therefore, should be considered only as a qualitative guide. In order to be more precise, 3D PIC calculations using the LSP code[26,27] were performed.

The spatial distribution of the normalized electron density, perturbed by a TM_{01} mode, 500 MW, 28 GHz, 0.4 ns MW pulse injected into 3D waveguides of different radii filled with a plasma of $2.5\times10^{10}\,cm^{-3}$ initial density, calculated by 3D PIC simulations, is presented in Fig. 14. The periodic density variation in the wake is of the same order of magnitude as that seen for the 10 GHz microwave source (Ref. 19). At the time chosen, 3 ns, the first compressed electron density region ($z \sim 29$–33 cm) in the wake follows the upstream edge of the microwave pulse's position. Two additional compressed density regions formed at earlier times are also seen further upstream. These results agree qualitatively with those obtained by the 1D model (see Fig. 12). However, 3D modeling shows significantly smaller density modulations, especially for bunches following the first one.

In Fig. 15, the density variation along the radial and axial directions is drawn for the cases presented in Fig. 14. One can see that a maximum in the density modulation can be obtained for the same waveguide radius as that seen in Fig. 13(b). Also, one can see in Fig. 15(a) that increasing the microwave power may lead to a decrease in the electron density modulation for a fixed plasma density similar to the results of the 1D model.

V. SUMMARY

The results of our experimental research and numerical studies show the successful generation of an ~1.2 GW, 28.6 GHz, ~0.4 ns-duration TM_{01} microwave pulse by an SR-BWO powered by a ~5 ns-duration, ~280 keV, ~1.7 kA electron beam guided through a slow wave structure by an 8 T external magnetic field. The results of a 1D analytical model and 3D LSP numerical simulations confirm that this microwave pulse can be used to

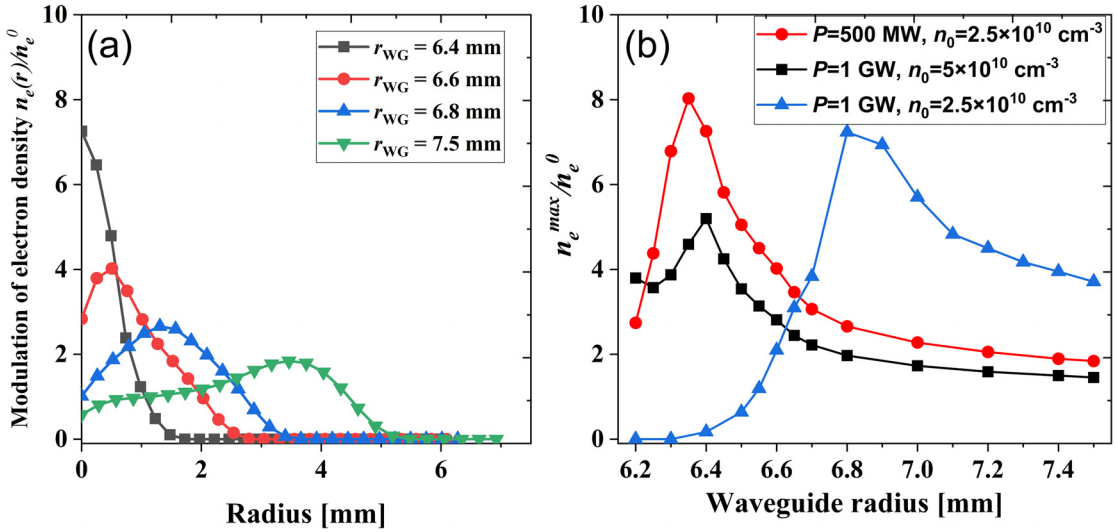

FIG. 13. (a) Radial distributions of the normalized density $n_e(r)/n_0^0$ for different waveguide radii for $P = 0.5$ GW and $n_e^0 = 2.5\times10^{10}\,cm^{-3}$. (b) Maximum electron density modulation n_e^{max}/n_e^0 vs. waveguide radius for $P = 1$ GW and $n_e^0 = 5\times10^{10}\,cm^{-3}$ (black squares), for $P = 500$ MW and $n_e^0 = 2.5\times10^{10}\,cm^{-3}$ (red circles), and for $P = 1$ GW and $n_e^0 = 2.5\times10^{10}\,cm^{-3}$ (blue triangles).

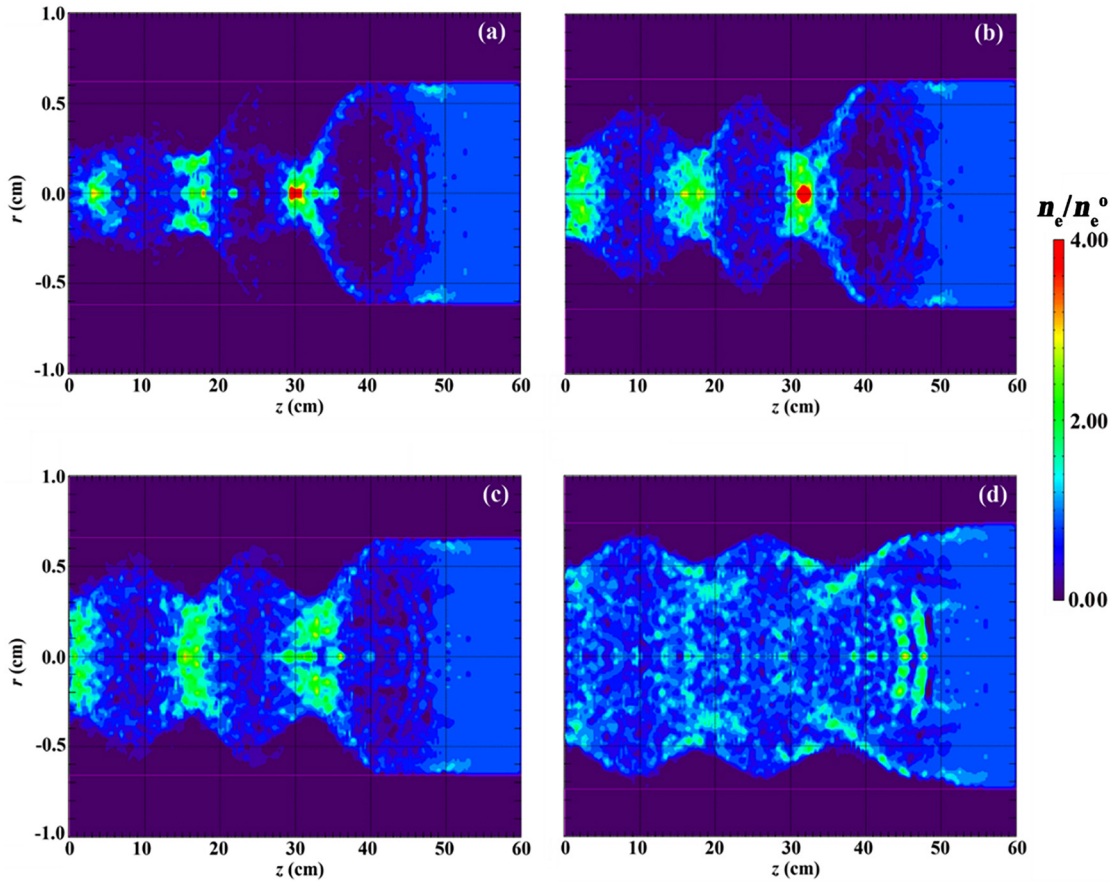

FIG. 14. Contours of the electron density n_e normalized to the initial density, $n_e^o = 2.5 \times 10^{10}$ cm^{-3} vs. z at 3 ns from the microwave pulse injection start time at $z = 0$, $t = 0$, for different waveguide radii 6.2 (a), 6.4 (b), 6.6 (c), and 7.5 mm (d) for 28 GHz, 500 MW, and 0.4 ns (FWHM) microwave pulses propagating from $z = 0$ downstream.

produce a measurable wakefield in a circular waveguide filled with plasma. The degree of the electron density modulation and radial location of these modulations can be controlled by the waveguide radius, microwave power, and plasma density. To form this preliminary plasma with controllable parameters being uniform along 60 cm, a flashboard array was developed and tested. The plasma parameters were characterized using various electrical, optical, and spectroscopic methods.

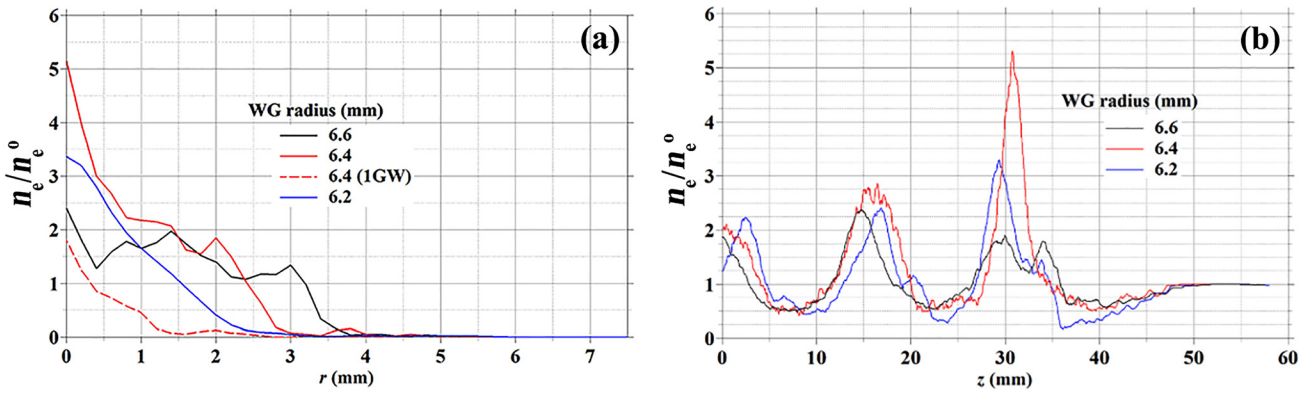

FIG. 15. The density variation of the normalized electron density along the radial and axial directions for the various waveguide radii of Fig. 14. (a) The density variation along r for a z value at the center of the first density concentration following the microwave pulse averaged over its width. (b) The density variation along z for $r = 0$, averaged over a 1 mm wide slice in r.

ACKNOWLEDGMENTS

The authors are grateful to E. Flyat and S. Gleizer for technical assistance and G. Shafir for fruitful discussions. This work was supported in part by the PAZY under Grant No. 2020960 and in part by the research program of the RAS #10.

REFERENCES

[1]V. V. Rostov, I. V. Romanchenko, M. S. Pedos, S. N. Rukin, K. A. Sharypov, V. G. Shpak, S. A. Shunailov, M. R. Ul'Masculov, and M. I. Yalandin, Phys. Plasmas **23**, 093103 (2016).
[2]P. Felsenthal, J. Appl. Phys. **37**, 4557 (1966).
[3]Y. L. Bogomolov, S. F. Lirin, V. E. Semenov, and A. M. Sergeev, JETP Lett. **45**(11), 680 (1987).
[4]A. L. Vicharev, V. B. Gildenburg, S. V. Golubev, B. G. Eremin, O. A. Ivanov, A. G. Litvak, A. N. Stepanov, and A. D. Yunakovskii, Sov. Phys. - JETP **67**, 724 (1988).
[5]V. B. Gildenburg, V. A. Krupnov, and V. E. Semonov, Sov. Tech. Phys. Lett. **14**, 738 (1988).
[6]S. P. Kuo, Phys. Rev. Lett. **65**, 1000 (1990).
[7]S. V. Bulanov, L. M. Kovrizhnykh, and A. S. Sakharov, Phys. Rep. **186**, 1 (1990).
[8]M. Brizhinev and A. Vikharev, Zh. Eksp. Teor. Fiz. **71**, 242 (1990).
[9]V. B. Gil'denburg, A. G. Litvak, and N. A. Zharova, Phys. Rev. Lett. **78**, 2968 (1997).
[10]H. K. Malik, S. Kumar, and K. P. Singh, Laser Part. Beams **26**, 423 (2008).
[11]A. K. Aria and H. K. Malik, Open Plasma Phys. J. **1**, 1 (2008).
[12]A. K. Aria and H. K. Malik, Opt. Commun. **282**, 423 (2009).
[13]G. Shafir, Y. E. Krasik, Y. P. Bliokh, D. Levko, Y. Cao, J. G. Leopold, R. Gad, V. Bernshtam, and A. Fisher, Phys. Rev. Lett. **120**, 135003 (2018).
[14]G. Shafir, Y. Cao, Y. Bliokh, J. G. Leopold, D. Levko, V. Rostov, R. Gad, A. Fisher, V. Bernshtam, and Y. E. Krasik, Phys. Plasmas **25**, 032308 (2018).
[15]Y. Cao, J. G. Leopold, Y. P. Bliokh, and Y. E. Krasik, Phys. Plasmas **25**, 103101 (2018).
[16]N. S. Ginzburg, N. Y. Novozhilova, I. V. Zotova, A. S. Sergeev, N. Y. Peskov, A. D. Phelps, S. M. Wiggins, A. W. Cross, K. Ronald, W. He, V. G. Shpak, M. I. Yalandin, S. A. Shunailov, M. R. Ulmaskulov, and V. P. Tarakanov, Phys. Rev. E: Stat. Phys., Plasmas, Fluids, Relat. Interdiscip. Top. **60**, 3297 (1999).
[17]S. D. Korovin, A. A. Eltchaninov, V. V. Rostov, V. G. Shpak, M. I. Yalandin, N. S. Ginzburg, A. S. Sergeev, and I. V. Zotova, Phys. Rev. E: Stat., Nonlinear, Soft Matter Phys. **74**, 016501 (2006).
[18]G. Shafir, D. Zolotukhin, V. Godyak, A. Shlapakovski, S. Gleizer, Y. Slutsker, R. Gad, V. Bernshtam, Y. Ralchenko, and Y. E. Krasik, Plasma Sources Sci. Technol. **26**, 2 (2017).
[19]Y. P. Bliokh, J. G. Leopold, G. Shafir, A. Shlapakovski, and Y. E. Krasik, Phys. Plasmas **24**, 063112 (2017).
[20]P. Gibbon, *Short Pulse Laser Interactions with Matter* (IMPERIAL COLLEGE PRESS AND DISTRIBUTED BY WORLD SCIENTIFIC PUBLISHING CO., 2005).
[21]Y. E. Krasik and A. Weingarten, IEEE Trans. Plasma Sci. **26**, 208 (1998).
[22]S. N. Rukin, Instrum. Exp. Tech. **42**, 439 (1999).
[23]G. Shafir, M. Kreif, J. Z. Gleizer, S. Gleizer, Y. E. Krasik, A. V. Gunin, O. P. Kutenkov, I. V. Pegel, and V. V. Rostov, J. Appl. Phys. **118**, 193302 (2015).
[24]G. A. Mesyats, *Explosive Electron Emission* (URO Press, Ekaterinburg, 1998).
[25]B. Goplen, L. Ludeking, D. Smith, and G. Warren, Comput. Phys. Commun. **87**, 54 (1995).
[26]D. R. Welch, D. V. Rose, B. V. Oliver, and R. E. Clark, Nucl. Instrum. Methods Phys. Res., Sect. A **464**, 134 (2001).
[27]D. R. Welch, D. V. Rose, M. E. Cuneo, R. B. Campbell, and T. A. Mehlhorn, Phys. Plasmas **13**, 063105 (2006).